SUPPLEMENTARY FIGURES

Figure S1. Repeatability of orbital telorism.

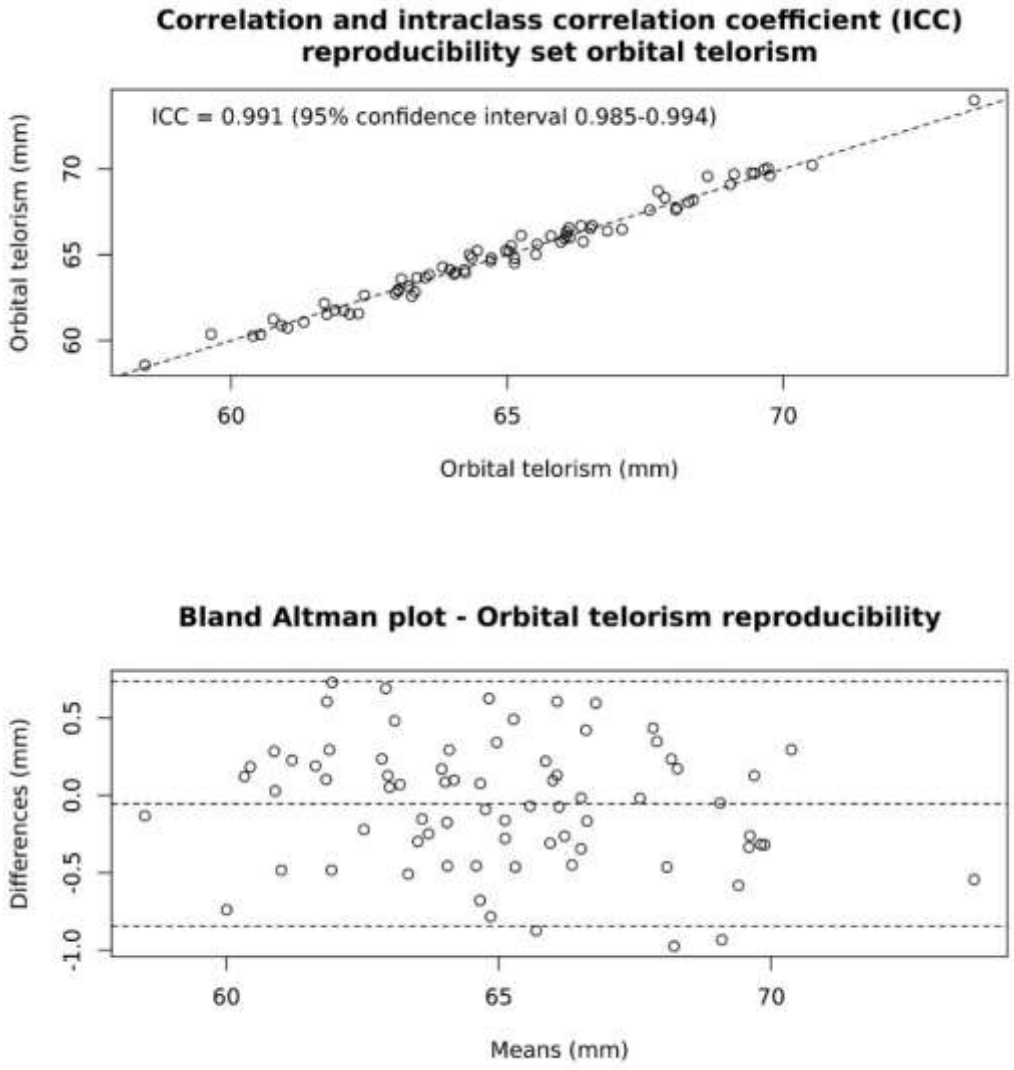

Plots showing the repeatability of orbital telorism in the Rotterdam Study repeatability subset (N = 85). A) Scatter plot showing the correlation between the orbital telorism measures of the two visits including the intraclass correlation coefficient (ICC) with 95% confidence intervals. B) Bland Altman plot showing the agreement between the two orbital telorism measurements for each individual. The x axis presents the mean paired measurement value, and the y axis presents the difference between the paired measurements, with 1.96 standard deviation from the mean depicted by dashed lines.

Figure S2. Repeatability of head width.

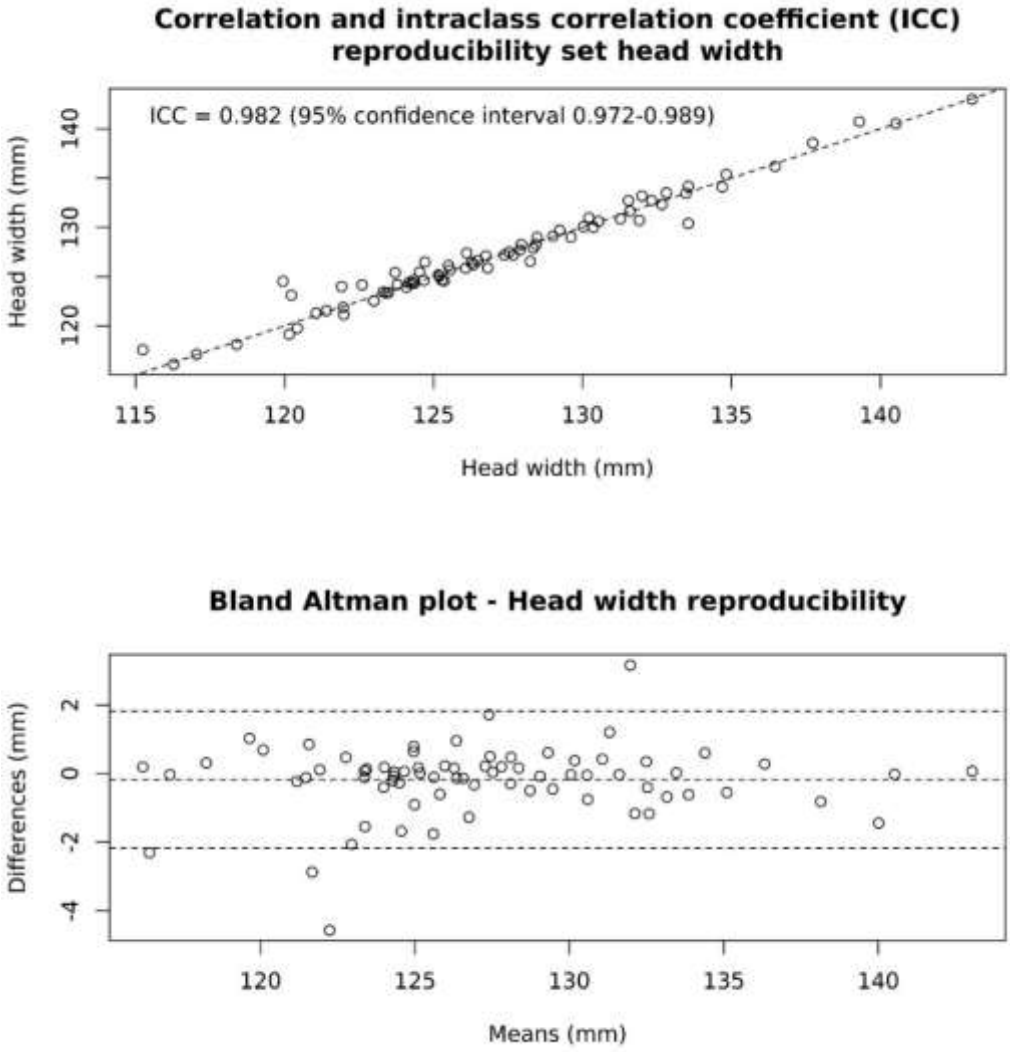

Plots showing the repeatability of head width in the Rotterdam Study repeatability subset (N = 85). A) Scatter plot showing the correlation between the head width measures of the two visits including the intraclass correlation coefficient (ICC) with 95% confidence intervals. B) Bland Altman plot showing the agreement between the two head width measurements for each individual. The x axis presents the mean paired measurement value, and the y axis presents the difference between the paired measurements, with 1.96 standard deviation from the mean depicted by dashed lines.

Figure S3. Correlation orbital telorism and interpupillary distance.

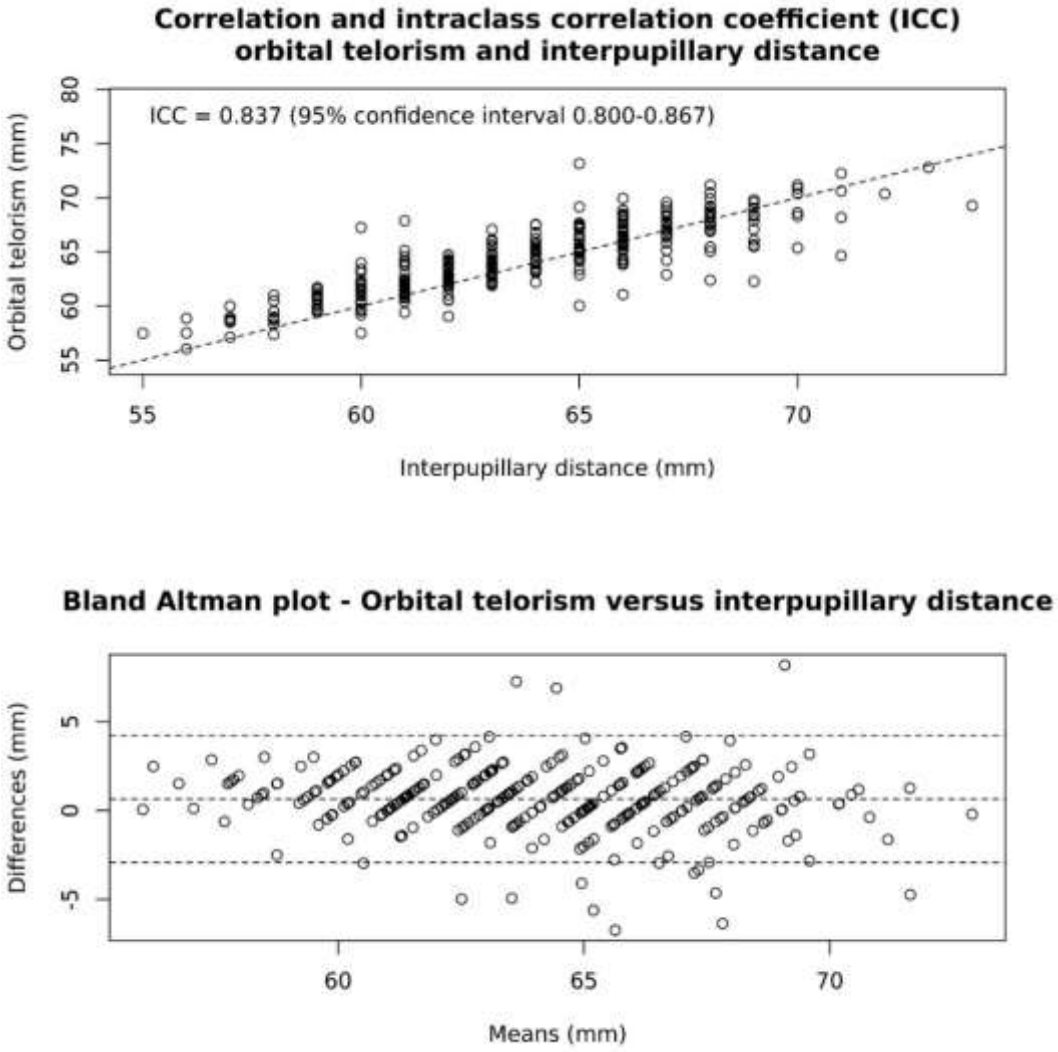

Plots showing the reproducibility of orbital telorism in the Rotterdam Study (N = 316), using interpupillary distance measures as a reference. A) Scatter plot showing the correlation between the orbital telorism and interpupillary distance values including the intraclass correlation coefficient (ICC) with 95% confidence intervals. B) Bland Altman plot showing the agreement between the orbital telorism and interpupillary distance measurement for each individual. The x axis presents the mean paired measurement value, and the y axis presents the difference between the paired measurements, with 1.96 standard deviation from the mean depicted by dashed lines.

Figure S4. Correlation of orbital telorism with potential confounders.

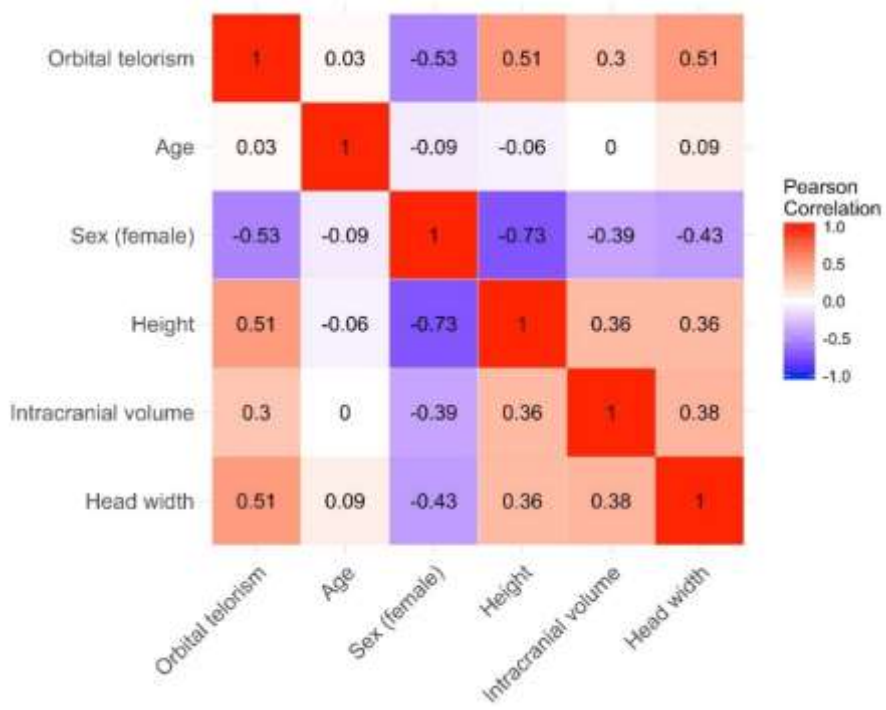

Heatmap showing the Pearson correlation coefficients for orbital telorism and the main covariates used across the different models, namely age, sex, height, intracranial volume and head width. Red depicts a positive correlation, blue a negative correlation. The Pearson correlation values are shown in the corresponding cells.

Figure S5. Polygenicity and discoverability.

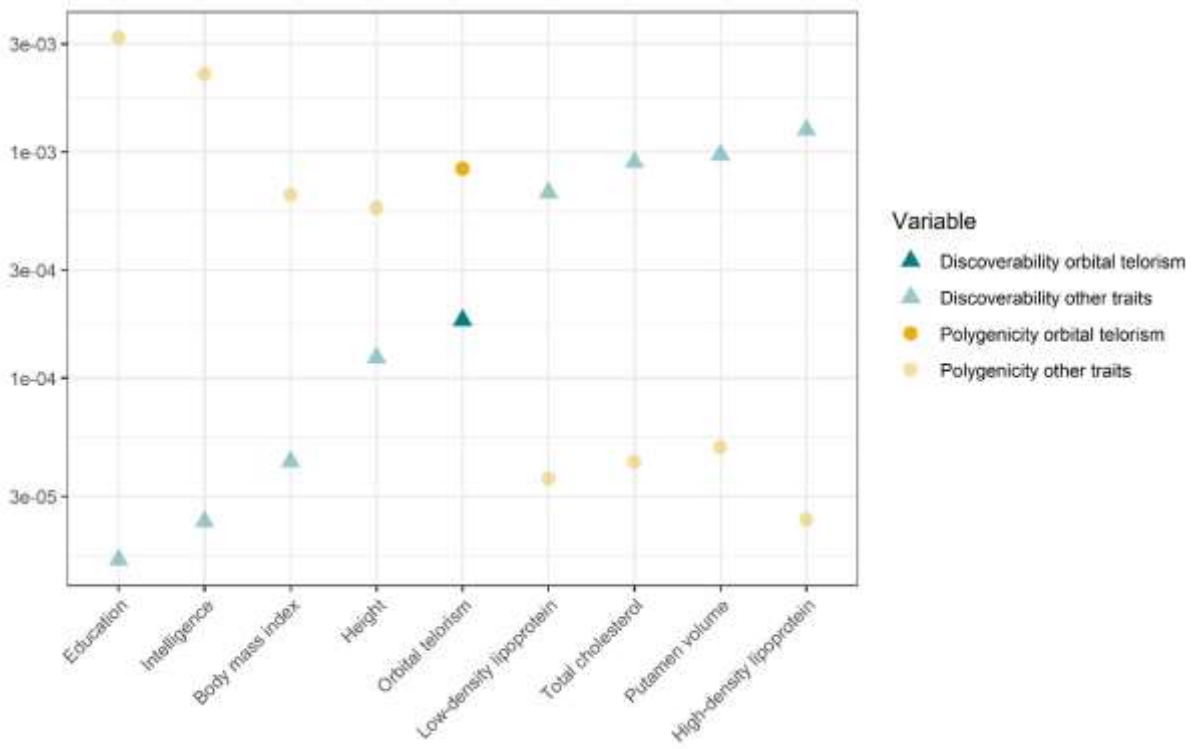

Scatter plot showing the polygenicity and discoverability estimates for orbital telorism, as well as other continuous traits as reported by Holland *et al.* (1). Polygenicity estimates are shown in yellow and discoverability estimates in blue, with more transparency for the non-telorism traits.

Figure S6. Replication results excluding genetic lead variants that replicated individually.

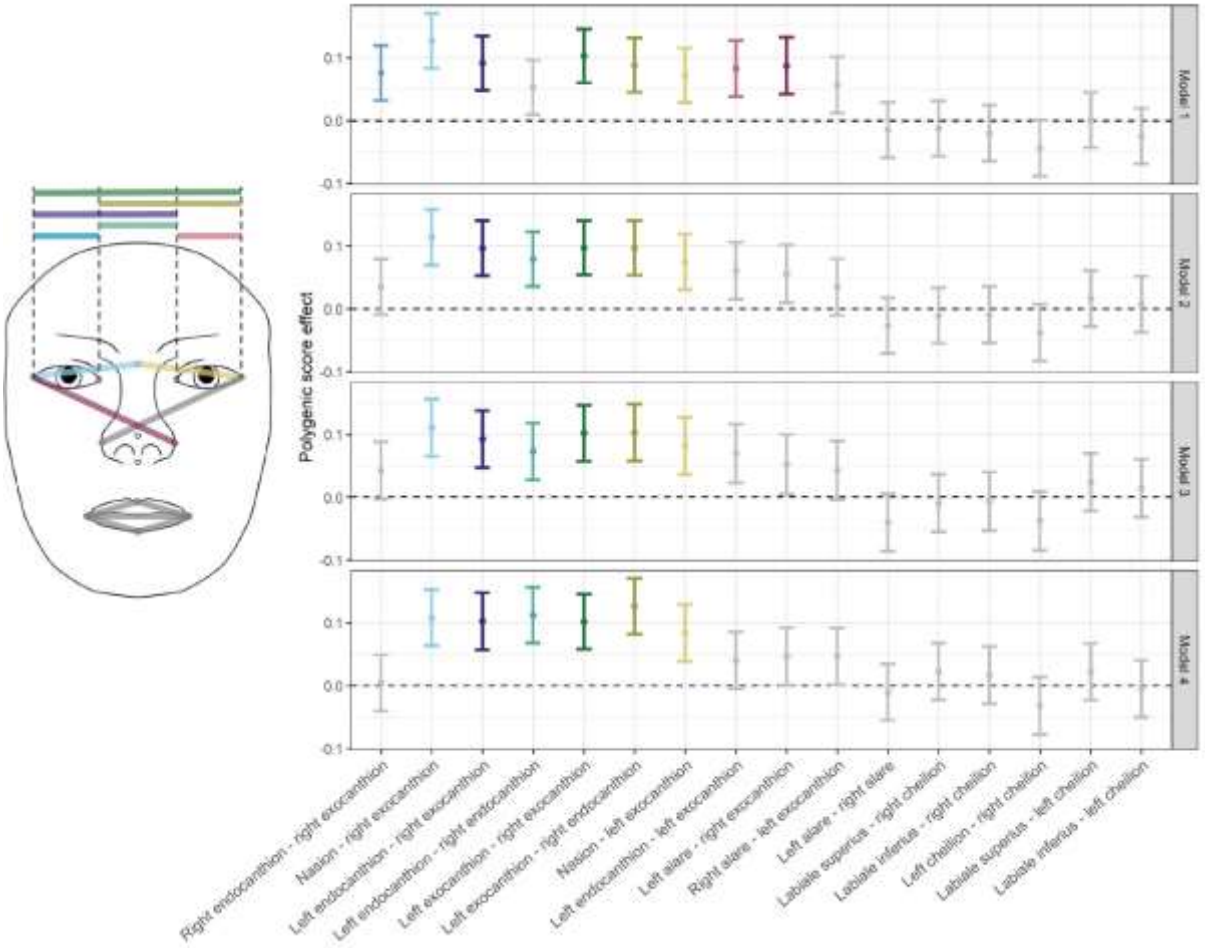

Plot showing the overall contribution of genetic lead variants to facial shape measures in the genome-wide association study by Xiong et al. (2) across the different models, while excluding genetic variants that replicated individually in this replication sample. Point estimates with their 95% confidence intervals are shown, with colored error bars depicting facial morphological distances surviving the Bonferroni multiple testing threshold ($P < 0.05/16$).

Figure S7. Replication results excluding Rotterdam Study samples.

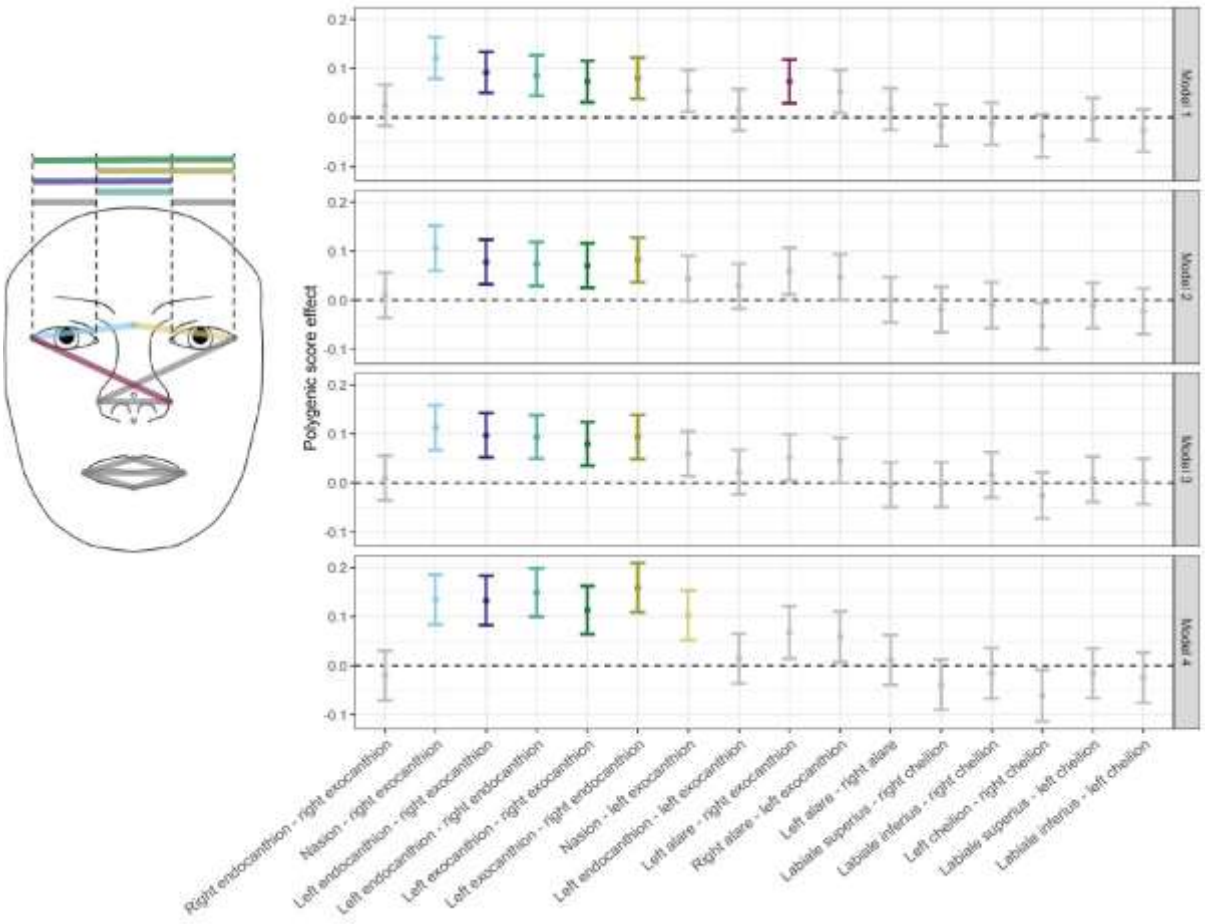

Plot showing the overall contribution of genetic lead variants to facial shape measures in the genome-wide association study by Xiong *et al.* (2) without the Rotterdam Study across the different models. Point estimates with their 95% confidence intervals are shown, with colored error bars depicting facial morphological distances surviving the Bonferroni multiple testing threshold ($P < 0.05/16$).

Figure S8. Receiver operation characteristic (ROC) curves for hypo- and hypertelorism with basic models including height and intracranial volume.

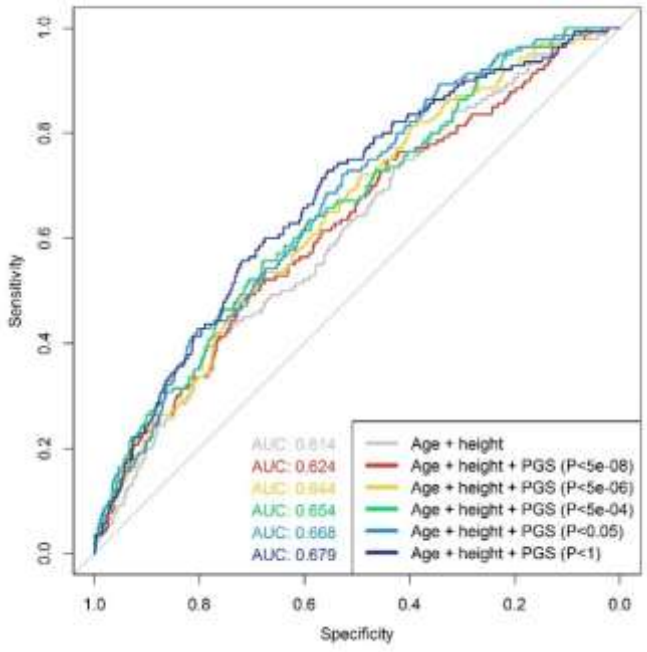

A)

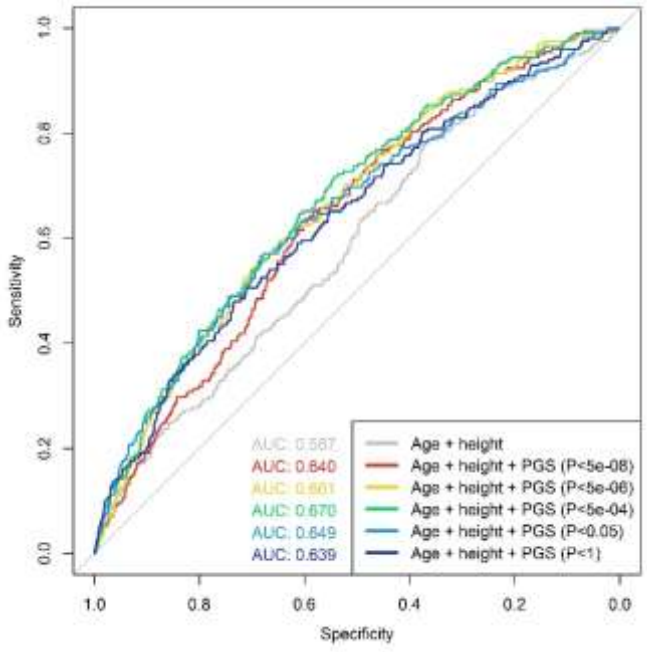

B)

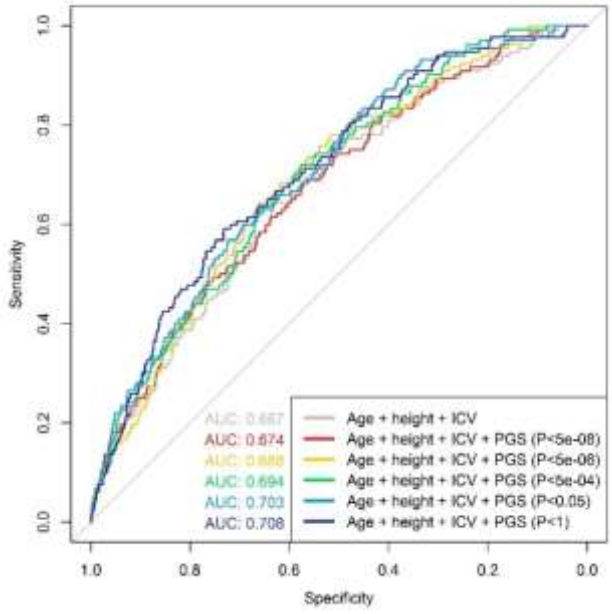

C)

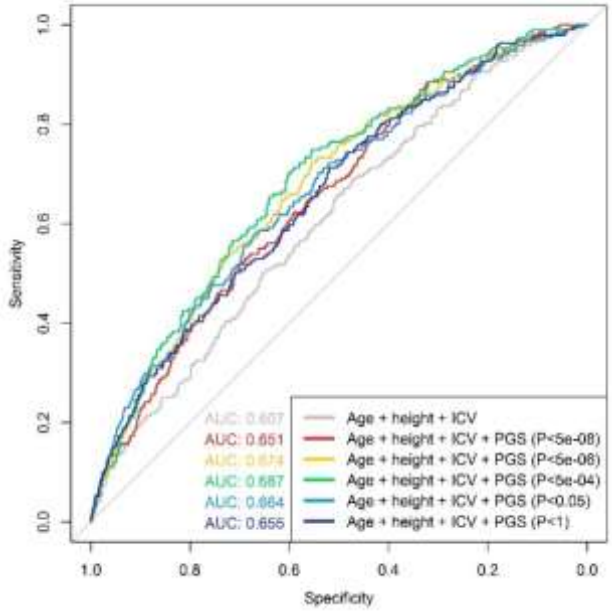

D)

Receiver operating characteristic (ROC) curves for the discriminative value of polygenic scores (PGS) for hypo- and hypertelorism. The curves present the area under the curve (AUC) of two basic prediction models, and the AUCs after adding PGS with different p-value thresholds for the inclusion of genetic variants. A) AUCs for hypotelorism with age and height in the basic model; B) AUCs for hypertelorism with age and height in the basic model; C) AUCs for hypotelorism with age, height and intracranial volume (ICV) in the basic model; D) AUCs for hypertelorism with age, height and ICV in the basic model.

REFERENCES

1 Holland, D., Frei, O., Desikan, R., Fan, C.-C., Shadrin, A.A., Smeland, O.B., Sundar, V.S., Thompson, P., Andreassen, O.A. and Dale, A.M. (2020) Beyond SNP heritability: Polygenicity and discoverability of phenotypes estimated with a univariate Gaussian mixture model. *PLoS Genet.*, **16**, e1008612-e1008612.

2 Xiong, Z., Dankova, G., Howe, L.J., Lee, M.K., Hysi, P.G., de Jong, M.A., Zhu, G., Adhikari, K., Li, D., Li, Y. *et al.* (2019) Novel genetic loci affecting facial shape variation in humans. *Elife*, **8**, e49898.